Advances in Science and Technology Research Journal

Advances in Science and Technology Research Journal, 2025, 19(10), 65–79
https://doi.org/10.12913/22998624/207834
ISSN 2299-8624, License CC-BY 4.0

Received: 2025.06.17
Accepted: 2025.08.15
Published: 2025.09.01

Evaluation of the force meter accuracy in the engineering industry applications

Krzysztof Tomczyk[1], Małgorzata Kowalczyk[2*], Tomasz Gębarowski[3], Csaba Felhő[4]

[1] Faculty of Electrical and Computer Engineering, Cracow University of Technology, Warszawska 24, 31-155 Krakow, Poland
[2] Faculty of Mechanical Engineering, Cracow University of Technology, al. Jana Pawła II 37, 31-864, Krakow, Poland
[3] Institute of Manufacturing Science, University of Miscolc, H-3515 Miskolc-Egyetemváros, Hungary
* Corresponding author's e-amil: malgorzata.kowalczyk@pk.edu.pl

ABSTRACT

This paper presents an assessment of the force meter (dynamometer) dynamic accuracy applied in the engineering industry. This assessment was made by determining the dynamic error based on the absolute error criterion. The mathematical basis for determining the dynamometers error was presented, and the corresponding procedures were developed. The values of dynamometer parameters and associated uncertainties were determined, then they were compared with the values calculated in the corresponding datasheet and finally the relationship between the dynamic absolute error and the dynamometer parameters was presented. The solutions presented allow the easy and quick determination of the accuracy of the dynamometers, and first of all significantly an increase the reliability and safety of engineering systems which use these type of measuring devices. The upper bound of the dynamic error developed in the paper may constitute an additional comparative criterion in assessing the accuracy of dynamometers produced by different manufacturers. New achievement of this paper is the presentation of the relationship between the dynamic error expressed by using the absolute error criterion and the values of the parameters of the mathematical model of the dynamometer in terms of applications in the engineering industry. These relationships are presented using the corresponding mathematical functions as well as graphically using 3D graphs. The calculation results were obtained using MathCad 5.0 and MATLAB R2024.

Keywords: force meter, upper bound of the dynamic error, cutting force.

INTRODUCTION

The force meter (dynamometer), as a device designed to measure forces or torques, is widely used in the engineering industry [1, 2]. This device is commonly applied in machining processes such as turning, milling, and drilling, where it enables precise measurement of cutting forces in multiple directions [3,4]. Such measurements allow for real-time monitoring and assessment of mechanical loads acting on the cutting tool and workpiece, which is essential for evaluating tool performance, process stability, and machining efficiency [5]. Dynamometers are often used in experimental setups to analyse the effects of cutting parameters – such as feed rate, cutting speed, and depth of cut–on force components and energy consumption [6]. They also support optimization of machining conditions, tool geometry, and cooling strategies to improve surface quality and reduce tool wear [7]. In research and industrial environments, cutting force measurements are essential for validating simulation models and for characterizing the machinability of advanced materials, including titanium alloys and shape memory alloys [8, 9].

In engineering practice, dynamometers are calibrated using the specialised measuring stations designed to reproduce tensile, compressive or shear forces [10, 11]. Most often, this involves point tests, for which the load realised is a percentage of the permissible load of the dynamometer

(e.g. 20%, 40%, 60%, 80% and 100% of the maximum load value) [12]. The readings of the calibrated device are compared with the readings of force standards [13]. The repeatability of the dynamometer readings for the measurement points carried out during calibration is also verified [14]. However, these are static tests that do not fully reflect the dynamic loads [15] that affect the dynamometer during measurements carried out in the actual operating conditions of the engineering infrastructure [16].

In order to increase the accuracy [17] of dynamometers, the paper proposes the procedure consisting of the assessment of the dynamic errors for this type of measuring devices [18–21]. This procedure is based on the results of the parametric identification [22] of the dynamometer, carried out in the conditions of a the real measurement experiment [23, 24]. The dynamometer is excited impulsively using the modal hammer [25], and its time response is recorded using dedicated measurement software, e.g. DynoWare or LabVIEW [26, 27]. Then, on the basis of the recorded results, the numerical procedure is carried out which is aimed at determining the parameters of the mathematical model (the transfer function) of the dynamometer [28]. Satisfactory modelling results [29] can be obtained by using the Monte Carlo method [30] or the Levenberg-Marquardt algorithm [31]. The first method is a randomised procedure based on the selected pseudorandom number generator, while the Levenberg-Marquardt algorithm is an iterative procedure implementing nonlinear optimisation by combining the steepest descent and Gauss-Newton methods. After determining the dynamometer model parameters, simulation and computational studies are carried out, aimed at determining the upper bound of the dynamic error in accordance with the assumed quality criterion [18–20]. The upper bound of the dynamic error is defined as the highest possible value of the dynamic error that may be obtained during the real dynamometer operation [18–20]. This error corresponds to the signal with constraints, also determined by computational and simulation methods [18, 19] which has a property such that only the lower value of the dynamic error can be obtained as a result of any other real dynamic signal contained in its constraints [18, 19]. The paper presents the research procedure aimed at determining the upper bound of the dynamic error (according to the absolute error criterion) and the corresponding signal with two constraints [18, 19]. These constraints concern the magnitude and the duration of the signal which is therefore rectangular in shape. The number of signal time-switchings (signal changes) and the time values corresponding to these switchings are determined by simulation way using the dedicated computation algorithm.

This paper presents examples of calculations of the upper bound of the dynamic error and the corresponding signal with constraints for the selected Kistler dynamometer of type 9257B and for x-axis [32]. Additionally, the values of the upper bound of the dynamic error were determined [18–20] for the grid of the dynamometer parameters which were assumed in advance, but around the parameters obtained on the basis of the parametric identification of the dynamometer. On this basis, the spatial (multivariate) regression of these points was performed and the corresponding functions were determined [33–36]. As a result, it is possible to determine the upper bound of the dynamic error by substituting into these functions any values of the dynamometer model parameters, without the need to implement numerical and computational procedures necessary to determine the above error.

The solutions presented in the paper are an extension of the results obtained based on traditional calibration methods, commonly used in engineering practice, by the special functions which allow to obtain the value of the upper bound of the dynamic error by easy way without the need to perform the complex numerical calculations. The upper bound of the dynamic error can be an additional comparative criterion when assessing the accuracy of dynamometers manufactured by different companies. However, determining the grid of points for multivariate regression require the implementation of parametric identification aimed at determining all parameters related to the mathematical model of the dynamometer, including the damping factor. This was achieved by using the parametric identification methods based on recording the step response of the dynamometer which is a function of time. Determining of these parameters, using the frequency response function (including both the amplitude and phase response with respect to frequency), would require exceeding the resonance frequency which would be associated with a high risk of damaging of the dynamometer.

The solutions presented here can contribute to the effective selection of dynamometers for

measurement applications in the engineering industry, based on the assessment of the dynamic errors. Therefore, a significant increase in the accuracy of measurements carried out using these devices can be achieved.

Next Section 2 of this paper presents the theoretical basis necessary to determine the upper bound of the dynamic error, as well as to carry out the spatial (multivariate) regression based on the calculation points for this type of error. Section 3 presents the research results for the Kistler dynamometer of type 9257B and determines the spatial functions representing the dynamic error for selected ranges of parameter variation for the mathematical model of the dynamometer. Section 4 presents the verification of the obtained results while Section 5 concerns the summary of the results obtained during the conducted research.

MATERIALS AND METHODS

The mathematical model of the dynamometer is defined by the transfer function as follows [19, 21]:

$$K_{\mathrm{d}}(s) = \frac{-a\omega_0^2}{s^2 + 2\omega_0\beta s + \omega_0^2} = \frac{-2\pi a\omega f_0^2}{s^2 + 4\pi f_0\beta s + 2\pi f_0^2} \tag{1}$$

where: *a[V/N]*, ω_0 *[rad/s]* and β [–] denote the static amplification factor, the pulsation of natural undamped vibrations and the damping factor, respectively, while s = jω denotes a Laplace operator and $\mathrm{j} = \sqrt{-1}$ is the imaginary number.

The parameters a, ω_0 and β in Equation 1 results from the following relations [19]:

$$a = m/k, \omega_0 = \sqrt{k/m}, \quad \beta = r/\left(2\sqrt{km}\right) \tag{2}$$

where: *m [kg]*, *k [N/m]* and *r [kg/s]* denote the mass, spring constant and dumping coefficient which are associated with the equivalent model of dynamometer.

As in most calibration procedures, to determine the upper bound of the dynamic error based on the model given by Equation 1, a reference model is necessary. An analogue filter of higher order can be efficiently applied as the reference model [19]. For simulation purposes, the eighth-order Butterworth filter was adopted in this paper. The mathematical model of this filter is given by the following transfer function:

$$K_{\mathrm{r}}(s) = \frac{a}{\alpha_1 + \alpha_2 + \alpha_3 + \alpha_4} \tag{3}$$

where: $\alpha_1 = \left(\frac{s}{\omega_{\mathrm{c}}}\right)^2 + 0.3728\,\frac{s}{\omega_{\mathrm{c}}} + 1,$

$\alpha_2 = \left(\frac{s}{\omega_{\mathrm{c}}}\right)^2 + 0.7202\,\frac{s}{\omega_{\mathrm{c}}} + 1,$

$\alpha_3 = \left(\frac{s}{\omega_{\mathrm{c}}}\right)^2 + 0.9754\,\frac{s}{\omega_{\mathrm{c}}} + 1,$

$\alpha_4 = \left(\frac{s}{\omega_{\mathrm{c}}}\right)^2 + 1.1112\,\frac{s}{\omega_{\mathrm{c}}} + 1$

$\omega_c = 2\ \pi f_c$, and f_c denotes the cut-off frequency which corresponds to the operating range of the dynamometer under consideration [19].

The cut-off frequency f_c of the filter should be determined so that it corresponds to the operating bandwidth of the dynamometer. This bandwidth results from the 3-decibel deviation of the amplitude-frequency response from its steady state [19, 21, 30].

The value of the parameter f_c is determined by solving the following equation:

$$a + \frac{a}{100\%}\Lambda = \frac{a}{\sqrt{\left[1 - \left(\frac{f_c}{f_0}\right)^2\right]^2 + 4\beta^2\left(\frac{f_c}{f_0}\right)^2}} \tag{4}$$

where: Λ denotes the percentage degree of deviation of the amplitude-frequency response *A(f)* from the value *A(0)*. Considering that solving this equation produces four values, the negative results are rejected for obvious reasons (the parameter f_c cannot have negative values), and the lower positive value obtained is assumed as the solution result [19, 21].

The upper bound of the dynamic error for assumed the absolute criterion, denoted below by *D* is calculated using the following formula:

$$D = \int_0^T |k(t)|\mathrm{d}t \tag{5}$$

where: *T* denotes the dynamometer test time, while *k(t)* is the time function given by the following formula:

$$k(t) = \mathcal{L}^{-1}[K_{\mathrm{d}}(s)] - \mathcal{L}^{-1}[K_{\mathrm{r}}(s)] \qquad (6)$$

where: $\mathcal{L}^{-1}$ denotes the inverse Laplace transform. The function *k(t)* is therefore the impulse response which is obtained as the difference between the impulse responses of the dynamometer and the impulse response of corresponding reference [18, 19].

The signal with two constraints (magnitude and time *T*) is determined using the following formula:

$$x_0(t) = a \cdot \mathrm{sgn}[k(T - t)] \qquad (7)$$

where: notation *sgn* denotes the signum function, and the following condition: $0 < t < T$is fulfilled [18, 19].

The magnitude of the signal $x_0(t)$ is equal to the value of parameter α of the dynamometer. The number of switchings of this signal is correlated with the number of zero crossings of the impulse response *k(t)*.

The time representation of dynamic error associated with the signal $x_0(t)$ defined by the convolution integral, as follows:

$$e(t) = \int_0^t k(t - \tau)\, x_0(\tau)\mathrm{d}\tau \qquad (8)$$

where: τ is the integration variable [18, 19].

The error *e(t)* has the highest possible value for $t = T$ which corresponds to the upper bound of the dynamic error. The error *e(t)* has the property that it always reaches its maximum value for the final time *T* which is characteristic of the absolute error criterion [18, 19]. Figure 1 shows the example error *e(t)*

RESULTS AND DISCUSSION

The results of parametric identification represent the values of the parameters:α, ω_0 and β of the transfer function $K_d(s)$ given by Equation 1. This identification was carried out using the measuring station equipped with the Kistler dynamometer of type 9257B, the modal hammer of type 086D05 and the measuring system with computers and DynoWare software version 3.1.2.0 which is used to record the impulse response of the dynamometer for the *x*-axis [27]. Two computers were used to facilitate the visualisation of the obtained results. Figure 2 shows the system applied for purpose of the parametric identification of the dynamometer.

The dynamometer was impacted directly into its housing using the modal hammer according to the *x*-axis and the corresponding impulse response was recorded. One hundred samples were recorded at times *t* equal to 0.014 s. The measurement points of the impulse response were selected in such a way that this response started from zero and ended when they achieved the steady-state [32]. The regression of the measurement points of the recorded impulse responses was performed using the Monte Carlo method and the Box-Muller pseudorandom number generator. The number of Monte Carlo trials carried out was equal to 2×10^5 [30]. The influence of environmental parameters (e.g. humidity, temperature) on the measurement conditions of the dynamometer impulse responses was not taken into account in this paper.

An analogous procedure to that shown in Figure 2 should be used in the case of impacting the dynamometer according to the *y*- and *z*- axes. In a similar way as for the *x*-axis, the corresponding impulse response measurement points should be recorded. However, in order to obtain consistency

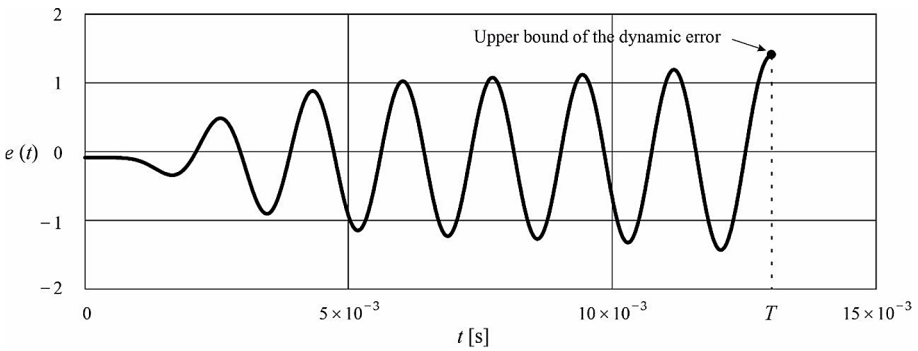

Figure 1. Example error *e(t)*

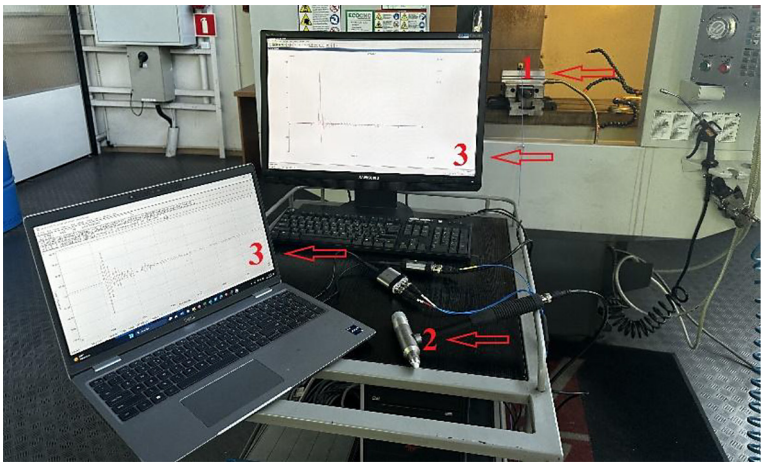

Figure 2. Measurement system applied for dynamometer parametric identification: 1 – dynamometer, 2 – impact hammer, 3 – computers equipped with DynoWare software

of the final results, an analogous method of approximating these measurement points (e.g. the Monte Carlo method) should be used.

Examples of measurement and simulation experiments for all three axes of the dynamometer using the Monte Carlo method are presented in [37].

Table 1 presents the results of regression carried out for the tested dynamometer for the *x*-axis. This Table contains the value of the parameters: α, ω_0 and β as well as the associated uncertainties: $u(a)$, $u\omega_0$ and $u\beta$

The values of the parameter ω_0 included in Table 1 differ from those reported in the datasheet [37]. These differences may be due to the fact that the identification of the dynamometer model based on the impulse response for the *x*-axis was aimed at determining also the parameter β related to the mathematical formula given by Equation 1 and not included in the corresponding datasheet. In order to compare the values of parameter α included in Table 1 and in the corresponding datasheet, there is a need to transform the unit pC/N to the unit V/N, as follows:

$$\frac{\mathrm{pC}}{\mathrm{N}} = \frac{\frac{\mathrm{pFV}}{\mathrm{N}}}{\mathrm{d_c} + \mathrm{c_c}} \tag{9}$$

where: the parameters d_c and c_c denote the dynamometer and connecting cable capacitances. The value of these parameters are equal to 220 pF and 100 pF for the Kistler dynamometer of type 9257B, respectively. Hence, based on Equation 9, we obtain

$$\frac{\mathrm{pC}}{\mathrm{N}} = \frac{1}{320}\frac{\mathrm{V}}{\mathrm{N}} \tag{10}$$

Recalculation of the value of parameter α included in Table 1 according to Equation 10, gives the value of this parameter tabulated in the corresponding datasheet [38], where the parameter α is equal to –7.5 pC/N.

The value of parameter β can be also obtained based on the data included in the datasheet [37], by involving the parameters called there as the sensitivity and overload. Late us denote by Δ_y the overload parameter. Than, we have

$$\beta = \left| \frac{-\ln\left(\frac{\Delta_y}{a}\right)}{\sqrt{\ln^2\left(\frac{\Delta_y}{a}\right) + \pi^2}} \right| \tag{11}$$

Substituting the value of parameters: α in V/N and Δ_y in kN included in the corresponding datasheet to Equation 11, we obtain: β = 0.975. Considering that the value of this parameter, similarly to the parameter ω_0 tabulated in Table 1, is different than the values included in the corresponding datasheet, below we check the compatibility of the parameters included in Table 1 and in the datasheet by comparing the 10% bandwidth for the corresponding amplitude responses, calculated by using the following formula

$$A(f) = \sqrt{K_\mathrm{d}(\mathrm{j}2\pi f)K_\mathrm{d}(-\mathrm{j}2\pi f)} \tag{12}$$

which involves the transfer function given by Equation 1.

Figure 3 shows the amplitude responses determined for the parameters: α, ω_0 and β tabulated in

Table 1. Value of parameter α, ω_0 and β s and associated uncertainties

x-axis		
Dynamometer parameters		
a [V/N]	ω_0 [rad/s]	β [–]
– 0.023	4410	0.3812
Associated uncertainties		
$u(a)$ [V/N]	$u(\omega_0)$ [rad/s]	$u(\beta)$ [–]
– 0.006	258	0.0039

Table 1 and obtained based on the corresponding datasheet. These responses have different shapes, but the same value of the cut-off frequency denoted by f_c which is equal to 220 Hz. The equality of the both cut-off frequencies can be considered as a confirmation of the correctness of determining the model parameters given by Equation 1 for the *x*-axis. It should also be emphasized that the cut-off frequency f_c is also important for the purpose of determining the upper bound of the dynamic error, according to Equation 5.

Based on the results included in Table 1, the values of the upper bound of the dynamic error and the corresponding signals $x_0(t)$ were determined.

Figure 4 shows the impulse responses: $k_d(t)$, $k_r(t)$ and $k(t)$ obtained for the parameters included in Table 1. The time T corresponds to the steady-state time of these responses and is equal to 0.025 s. The parameter f_c, calculated based on Equation 4, is equal to 258 Hz.

The impulse response $k(t)$ shown in Figure 4 was determined based on Equation 6, while the impulse responses $k_d(t)$ and $k_r(t)$ were obtained by using the following formulae:

$$k_{\mathrm{d}}(t) = \mathcal{L}^{-1}[K_{\mathrm{d}}(s)]$$
$$k_{\mathrm{r}}(t) = \mathcal{L}^{-1}[K_{\mathrm{r}}(s)] \tag{13}$$

From Figure 4, it follows that the impulse response $k_d(t)$ has a steady state of about 0.005 s, while this time for the impulse responses $k_r(t)$ and $k(t)$ has a much higher value which corresponds to the time T.

Figure 5 shows the signal $x_0(t)$ and error $e(t)$ obtained for the parameters tabulated in Table 1 The signal $x_0(t)$ shown in this Figure has 13

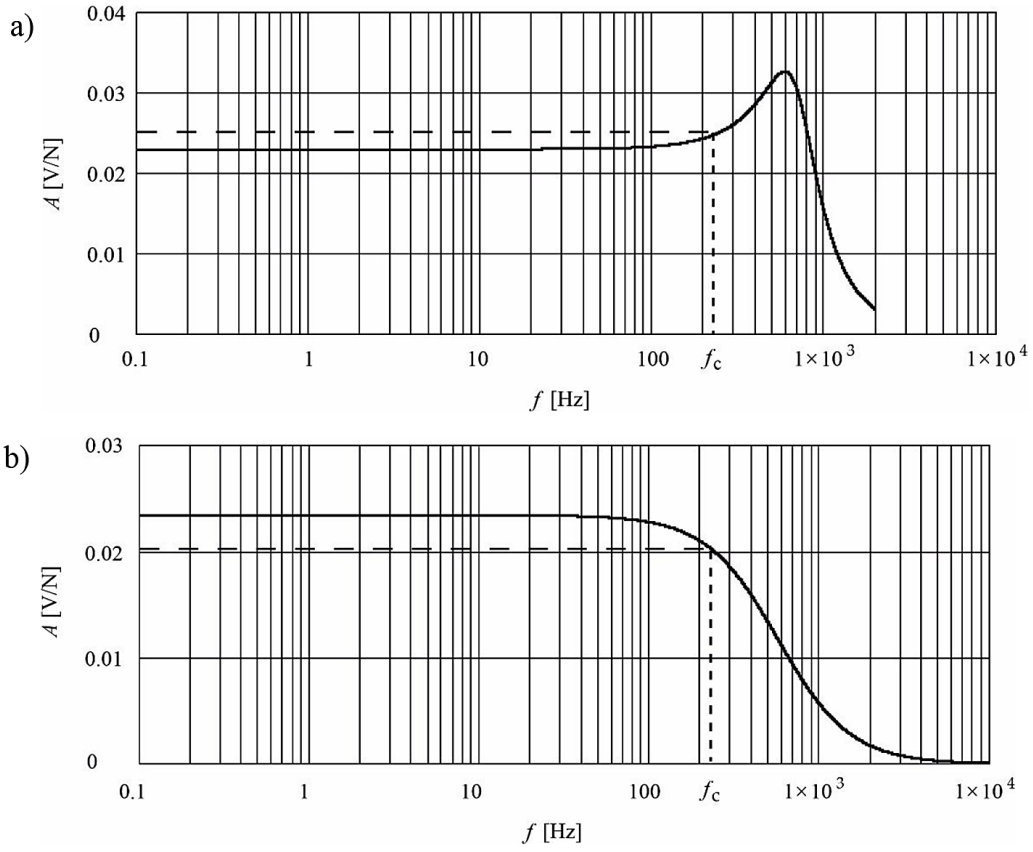

Figure 3. Amplitude responses determined for parameters tabulated in Table 1 (a) and obtained based on the datasheet (b)

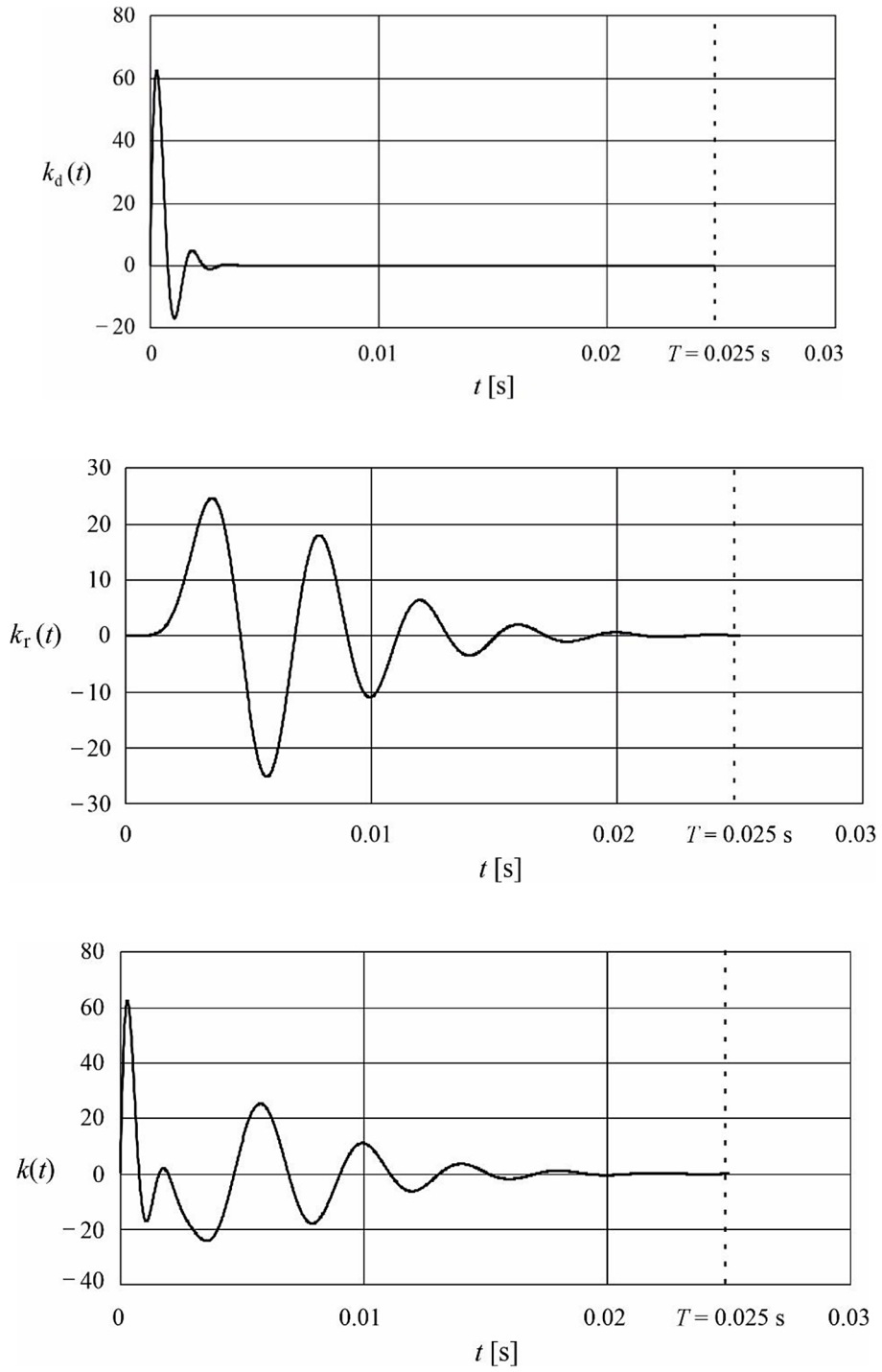

Figure 4. Impulse responses: $k_d(t)$, $k_r(t)$ and $k(t)$

time-switchings, and its essential property is that for any other signal contained within its constraints, we can obtain the error D of a value that is lower than or equal to the error obtained for the signal $x_0(t)$ [18,19]. The error $e(t)$ shown in this Figure increases with successive deviations from the value equal to zero up to a value t equal to T, where this error reaches its highest value. This error has six positive and five negative deviations. The error D given by Equation 5 is equal to 3.96×10^{-3} Vs. Figures 4–5 were developed using MathCad 5 software.

The 3D graphs and functions showing the relationship between the error D and the parameters α and β for ω_0 equal to 4000 and 5000 rad/s are presented below. It has been shown that the influence of changing the parameter ω_0 on the error values D is minimal and depends on the accuracy

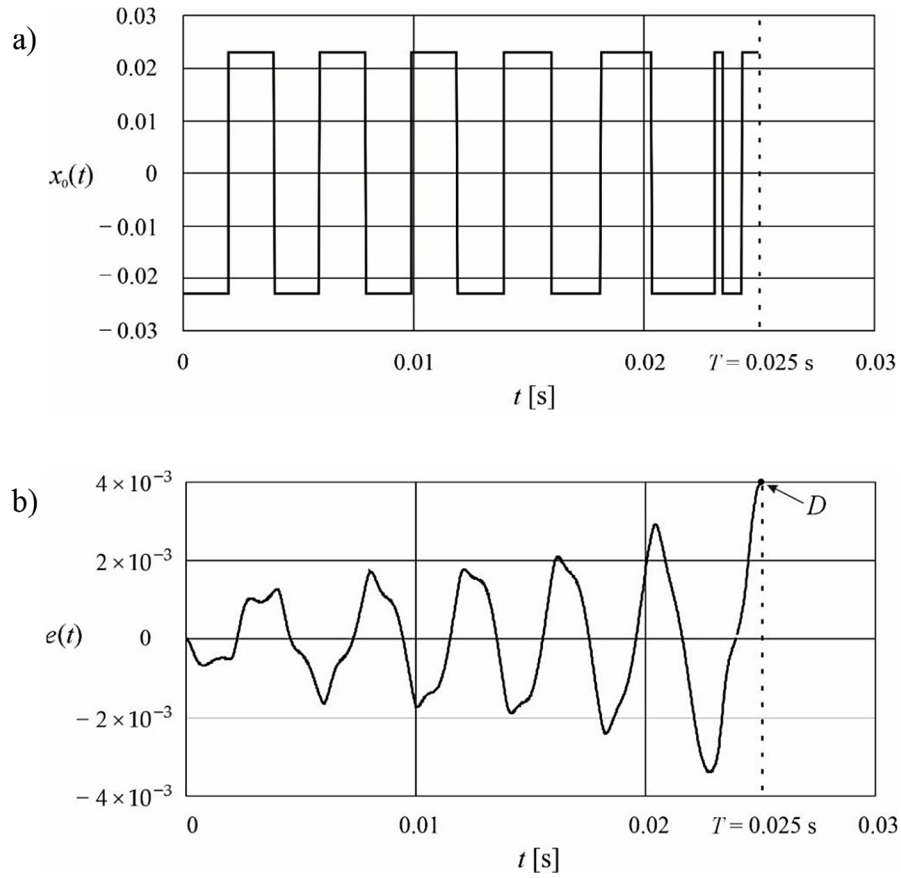

Figure 5. Signal $x_0(t)$ (a) and error e(t) (b)

of the performed calculations. The values of the parameters α and β for the 3D analysis were selected based on the results presented in Table 1. The test ranges for the parameters α was assumed to be from 0.01 to 0.05, with a step of 0.01 and for the parameter β were was assumed to be from 0.1 to 0.5, with a step of 0.1.

Table 2 presents the values of the parameter f_c determined based on Equation 4 and for the parameter β from the above assumed range, i.e. from 0.1 to 0.5. It should be emphasised that the parameter f_c does not change with changes in the parameter α. Considering that the time T of the steady state of the impulse response *k(t)* depends on the parameter f_c, the last row of Table 2 presents the values for this time. These values are 0.025 s and 0.020 s for frequency f_c equal to *4000 rad/s* and *5000 rad/s*, respectively.

Based on the data presented in Table 2, it can be easily seen that the value of the parameter f_c increases as the parameters β and ω_0 increase.

The values of the error *D* determined for the parameter α within the range of 0.01 to 0.05 with a step of 0.01 and parameter β within the range of 0.1 to 0.5 with a step of 0.1 for frequency f_c equal to 636.6 Hz and 795.8 Hz, respectively, are tabulated in Table 3.

Based on the data included in Table 3, it can be seen that the values of the error D for the parameter ω_0 equal to 4000 and 5000 rad/s are very close to each other for analogous values of the parameters α and β. Hence, the values of the error D were determined only for two values of the parameter ω_0.

The relationship between the error *D* given and the parameters α and β for ω_0 equal to 40*00 rad/s* is represented by the polynomial equation of the third order given by the following formula:

$$D(a,\beta) = -0.080 + 117.1 \cdot a - \\ -6.36 \cdot \beta + 1.06 \cdot 10^4 \cdot a^2 - \\ - 984.8 \cdot a \cdot \beta + 49.0 \cdot \beta^2 + \\ +1333 \cdot a^3 - 7857 \cdot a^2 \cdot \beta + \\ +1640 \cdot a \cdot \beta^2 - 75.83 \cdot \beta^3 \quad (14)$$

where: the sum of squared errors (SSE) of the approximation is equal to 0.53, while the root mean square error (RMSE) is 0.19.

Table 2. The values of the parameter f_c for the *x*-axis

ω_0 [rad/s]			
	4000	5000	
β [−]	0.1	194.1	242.6 242.6
	0.2	201.0	251.3
	0.3	214.7	268.3
	0.4	240.4	300.5
	0.5	301.0	376.2
	T [s]	0.025	0.020

The relationship between the error D given and the parameters α and β for ω_0 equal to *5000 rad/s* is represented by the polynomial equation of the third order given by the following formula:

$$D(a,\beta) = -0.09 + 112.2 \cdot a - \\ - 5.79 \cdot \beta + 1.08 \cdot 10^4 \cdot a^2 - \\ - 956.7 \cdot a \cdot \beta + 46.0 \cdot \beta^2 + \\ + 7.92 \cdot 10^{-10} \cdot a^3 - 80.29 \cdot a^2 \cdot \beta + \\ +1610 \cdot a \cdot \beta^2 - 71.83 \cdot \beta^3 \quad (15)$$

where: the SSE and RMSE are equal to 0.43 and 0.17, respectively.

Based on the analysis of the values of the SSE and RMSE, it can be easily noticed that slightly lower values of these parameters (by about 19% and 11%, respectively) were obtained for the function given by Equation 15.

The functions given by Equations 14 and 15 make it possible to determine the error D for any values of the parameters α and β in the range 0.1 to 0.5 and for the parameter ω_0 equal to 4000 and 5000 rad/s, respectively, without the need to use the computational procedure given by Equations 4–8. This accelerates and, above all, simplifies the calculation of the error D given by Equation 5.

Figures 6 (a) and (b) correspond to Equations 14 and 15 and show the 3D charts which represent the relationship between the error D given by Equation 5 and the parameters α and β for ω_0 equal to 4000 rad/s (Figure 6a) and 5000 rad/s (Figure 6b). These Figures were obtained using MATLAB R2024 software.

The grids of computational points which are presented in Figure 6 (a) and (b) were obtained by performing the numerical calculations using Equations 1–8. The functions given in Equations 13 and 14 allow determining the upper bound of the dynamic error for intermediate points with respect to the points of both grids. Based on these functions, one can easily determine the values of parameters α and β for the intervals shown in Figure 6 which are considered symmetrically around the parameters as tabulated in Table 1, and obtained on the basis of the implementation of the parametric identification procedure.

Table 3. Values of error D [Vs] · 10^{-3}

$\omega_0 = 4000$ rad/s, $T = 0.025$ s						
		β [−]				
		0.1	0.2	0.3	0.4	0.5
a [V/N]	0.01	1.06	0.87	0.79	0.74	0.72
	0.02	4.22	3.46	3.15	2.96	2.89
	0.03	9.50	7.79	7.08	6.66	6.50
	0.04	16.9	13.8	12.6	11.8	11.6
	0.05	26.4	21.6	19.7	18.5	18.1
$\omega_0 = 5000$ rad/s, $T = 0.020$ s						
		β [−]				
		0.1	0.2	0.3	0.4	0.5
a [V/N]	0.01	1.06	0.87	0.79	0.74	0.72
	0.02	4.25	3.48	3.16	2.97	2.89
	0.03	9.55	7.84	7.11	6.67	6.50
	0.04	17.0	13.9	12.6	11.9	11.6
	0.05	26.5	21.8	19.8	18.5	18.1

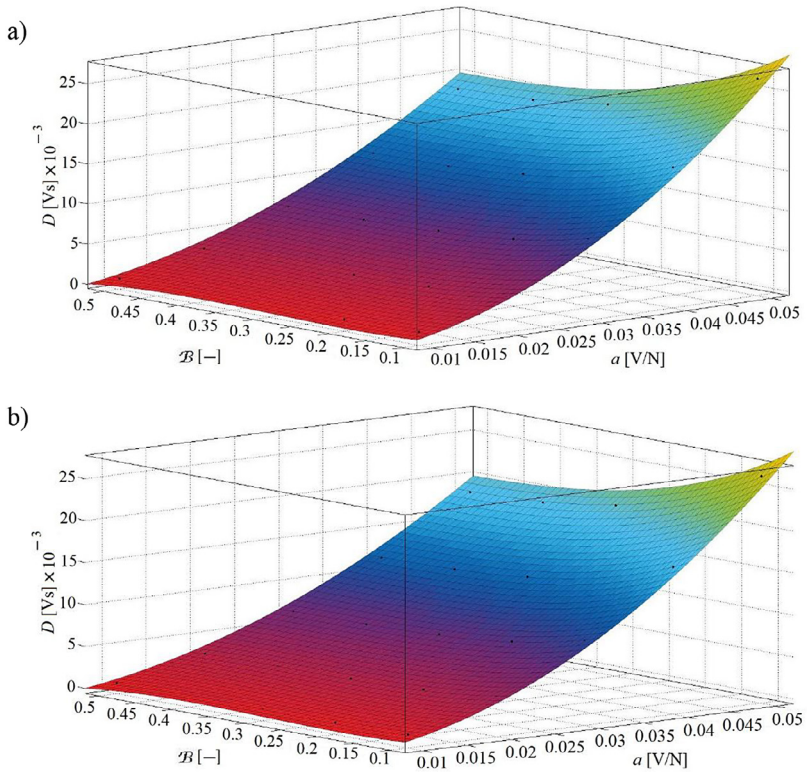

Figure 6. Relationship between the error *D* and the parameters α and β for $\omega_0 = 4000\ rad/s$ (a) and $\omega_0 = 5000\ rad/s$ (b)

RESULTS VERIFICATION

The verification of the functions given by Equations 14 and 15 and shown in Figure 6 is presented below. This verification consists in substituting selected values between the points listed in Table 3 into these functions. Additionally, it has been shown that any signal contained in the constraints of the signal $x_0(t)$gives an error *D* of a value lower than the error corresponding to the signal with constraints.

Table 4 includes the results of the verification of the function given by Equations 14 and 15. The values of error D were determined based on the intermediate points for those given in Table 3 and by substituting them into Equation 14 and 15.

The data presented in Table 4 confirm the correctness of the error determination based on Equations 14 and 15. For both function cases, the errors have values intermediate between those given in Table 3. The verification presented in Table 4 shows that the error values *D* can be determined quickly and easily without the need to apply complex calculation methods.

Figure 7 shows the signal $x_0(t)$ determined for the parameters: α = 0.015 N/V, β = 0.25 and $\omega_0 = 4000\ rad/s$ i.e. for those included in Table 4.

Signal $x_0(t)$ shown in Figure 5 has the following switching's: 0.0022 s, 0.0049 s, 0.0075 s, 0.0102 s, 0.0139 s, 0.0158 s, 0.0187 s, 0.0226 s, 0.0233 s, 0.0241 s and 0.0250 s. Based on these switching's, the polynomial function $p(t)$ with switching times corresponding to the switching of the signal $x_0(t)$ was developed. This function is:

$$\begin{aligned} p(t) = {} & -t^{13} + 0.174 \cdot t^{12} - \\ & 0.013 \cdot t^{11} + 0.609 \cdot 10^{-3} \cdot t^{10} - \\ & - 0.018 \cdot 10^{-3} \cdot t^{9} + 3.61 \cdot t^{8} \pm \\ & \pm 5.03 \cdot t^{7} + 4.86 \cdot t^{6} - 3.19 \cdot t^{5} + \\ & + 1.37 \cdot t^{4} - 3.53 \cdot t^{3} + 4.66 \cdot t^{2} - 2.11 \cdot t \end{aligned} \tag{16}$$

Let us use the function $p(t)$ as the verification signal $x_v(t)$, contained in the constraints of the signal $x_0(t)$.

Additionally, the signal $x_v(t)$ was rescaled in such a way that its magnitude was as close as possible to the magnitude constraint of the signal $x_0(t)$. This rescale is 3×10^{25}.

Figure 8 shows the signals $x_0(t)$ and $x_v(t)$. The error $e(t)$ that corresponds to the signal $x_v(t)$ is calculated using the following formula

Table 4. Values of error D [Vs] · 10^{-3}obtained using the functions given by Equations 14 and 15

$\omega_0 = 4000$ rad/s, $T = 0.025$ s						
		β [−]				
		0.1	0.2	0.3	0.4	0.5
a [V/N]	0.01	1.06	0.87	0.79	0.74	0.72
	0.02	4.22	3.46	3.15	2.96	2.89
	0.03	9.50	7.79	7.08	6.66	6.50
	0.04	16.9	13.8	12.6	11.8	11.6
	0.05	26.4	21.6	19.7	18.5	18.1
$\omega_0 = 5000$ rad/s, $T = 0.020$ s						
		β [−]				
		0.1	0.2	0.3	0.4	0.5
a [V/N]	0.01	1.06	0.87	0.79	0.74	0.72
	0.02	4.25	3.48	3.16	2.97	2.89
	0.03	9.55	7.84	7.11	6.67	6.50
	0.04	17.0	13.9	12.6	11.9	11.6
	0.05	26.5	21.8	19.8	18.5	18.1

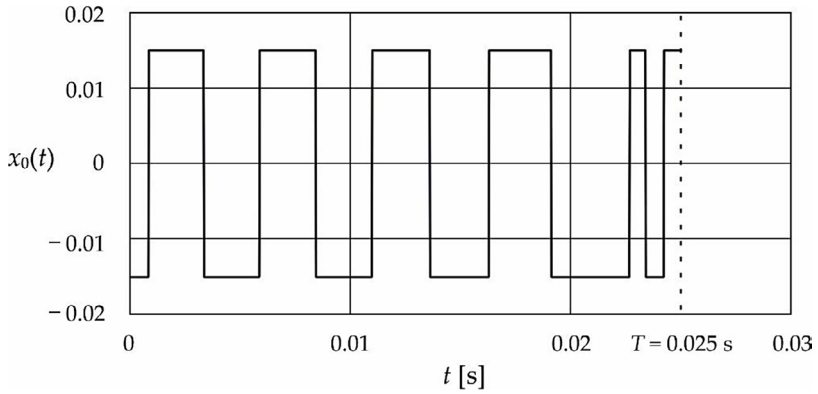

Figure 7. Signal $x_0(t)$ during verification

$$e_{\mathrm{V}}(t) = \int_0^t k(t-\tau)\, x_{\mathrm{v}}(\tau)\mathrm{d}\tau \tag{17}$$

Figure 9 shows the error $e_v(t)$ which maximum value denoted below by D_v is the equivalent of the error D.

The error D_v represents the maximum value of the error $e_v(t)$ which is equal to 2.77 × 10^{-4}. It is easy to notice that this value is definitely lower than the error presented in Table 4 and obtained for the above-considered parameters of the mathematical model of dynamometer. This confirms that each signal contained in the constraints of the signal $x_0(t)$ produces the error with the values lower than the error corresponding to the signal $x_0(t)$.

Below, the upper bound of the dynamic error D obtained for the dynamometer parameters as follow: $\alpha = 0.01$ *V/N*, $\beta = 0.01$ and $\omega_0 = 4000$ *rad/s* is compared with the corresponding error denoted below by symbol D_0 and determined based on the simpler formula, as follow

$$D_0 = \max\left[\int_0^t k(t-\tau)x_{\mathrm{t}}(\tau)\,\mathrm{d}\tau\right] \tag{18}$$

where:

$$x_{\mathrm{t}}(t) = a \cdot \sin(\omega_0 t) \tag{19}$$

while k(t) is determined based on Equation 6 and $x_t(t)$ denotes the special testing signal correlated with the dynamometer parameters α and ω_0 [19].

The value of error D tabulated in Table 3 is equal to 1.06 · 10^{-3} Vs, while the error D_0

calculated based on Equation 18 is $5.08 \cdot 10^{-4}$Vs. This means that the difference between the above errors is 47.9%. Considering that the error D is determined based on the maximizing signal $x_0(t)$, this percentage value increases the accuracy of determining the upper bound of the dynamic error based on the procedures presented in the paper.

Figure 10 shows the visual comparison between the error $e(t)$ shown in Figure 5 and the error $e_0(t)$ calculated based on the following formula

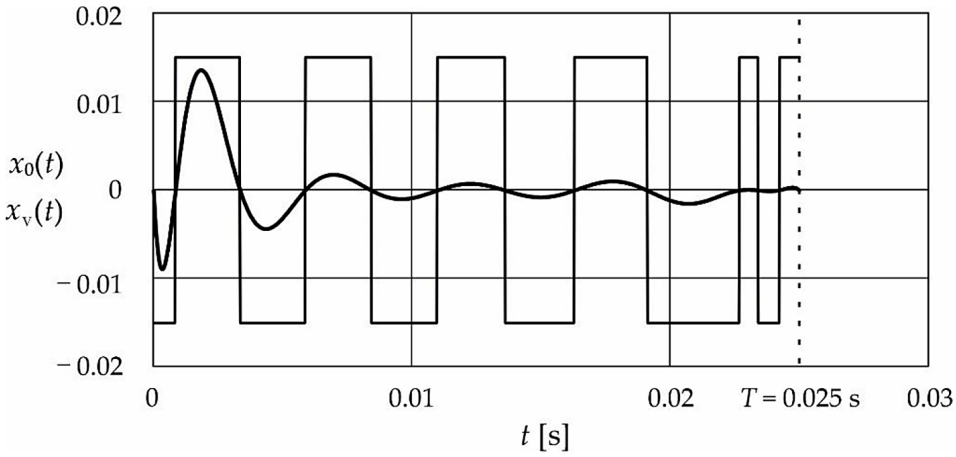

Figure 8. Signals $x_0(t)$ and $x_v(t)$

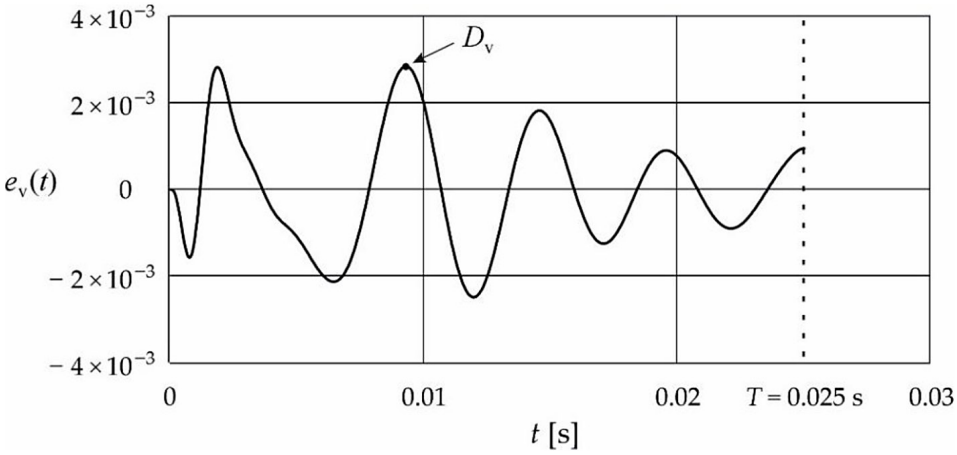

Figure 9. Error $e_v(t)$

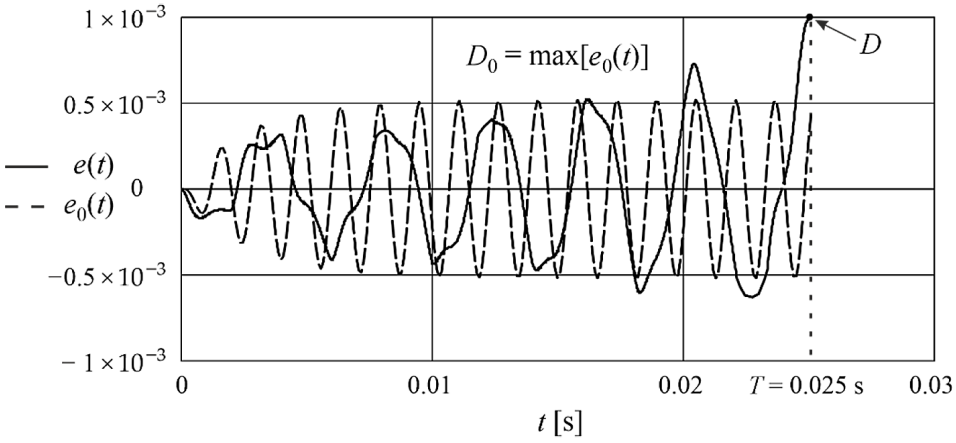

Figure 10. Comparison between the errors $e(t)$ and $e_0(t)$

$$e_0(t) = \int_0^t k(t-\tau)x_t(\tau)\,\mathrm{d}\tau \qquad (20)$$

which is correlated with the formula given by Equation 19.

It is easily seen from Figure 10 that the error *e(t)* gradually increases until it reaches a maximum value corresponding to the upper bound of the dynamic error *D*, while the error $e_0(t)$ reaches a stabilized value equal to an approximately the value of error D_0 for the time $t = 0.08\ s$.

CONCLUSIONS

The results obtained in this paper, confirm that in the case of force meters (dynamometers), it is possible to determine the upper bound of dynamic error which constitute the highest possible value of the error. The values of such errors can be used as a reliable criterion intended both for assessing the accuracy of individual dynamometers and for the mutual comparison of a larger number of such devices.

The consistency of the dynamometer parameters obtained using parametric identification and the corresponding datasheet was confirmed by checking the bandwidth. For both cases, an analogous cut-off frequency value equal to 220 Hz was obtained. The functions obtained by the spatial regression of the calculation points for the upper bound of the dynamic error confirm that they can be a very useful tool in assessing the accuracy of dynamometers in engineering applications. These functions are the new solution in the field of analysis of the dynamometers dynamic error and allow for the easy and fast determination of the upper bound of the dynamic error for any values of the parameters α (static amplification factor) and β (damping factor) related to the mathematical model of the dynamometer, without the need to apply dedicated calculation algorithms. Additionally, research carried out in this paper shows that the value of the dynamic absolute error obtained for the testing signal is about 50% less than the upper bound of the dynamic error.

The upper bound of the dynamic error is the highest value of the dynamic error that can be obtained during the operation of the dynamometer. This error applies to both the cutting forces and the results of recorded during measuring the other forces, e.g. roughing and finishing turning. The upper bound of the dynamic error is therefore a reference to the dynamic errors arising during measurements of various types of forces and can be treated as an equivalent to the accuracy class applicable during static measurements (the input signal has a defined shape in advance).

The limitation of the proposed method is determination of the relationship between the upper bound of the dynamic error and only two parameters of the dynamometer model. This limitation could be eliminated by using the neural networks in the future of research work.

Acknowledgements

This research was conducted at the Faculty of Electrical and Computer Engineering, Cracow University of Technology, and was financially supported by the Ministry of Science and Higher Education, Republic of Poland (grant no. E–1/2024).

REFERENCES

1. Martyr, A.J., Rogers, D. R.; Dynamometers: the measurement and control of torque, speed, and power. Elec., Hybrid, IC Eng., & Power Storage. 2021, 235–263, https://doi.org/10.1016/B978-0-12-821226-4.00009-7
2. Del-Cuerpo, I.; Mayorga, D.J. and Floody, P.D. Test–retest reliability of the functional electromechanical dynamometer for squat exercise. Int. J. Environ. Res. Public Health. 2023, 20, 1–13, https://doi.org/10.3390/ijerph20021289
3. Biruk-Urban, K, Józwik, J. Bere, P.; Cutting Forces and 3D Surface Analysis of CFRP Milling. Advances in Science and Technology Research Journal. 2022, 16(2), 206–215, https://doi.org/10.12913/22998624/147338
4. Kowalczyk, M. Analysis of cutting forces and geometric surface structures in the milling of NiTi alloy. Materials. 2024, 17(2), 1–17, https://doi.org/10.3390/ma17020488
5. Xing, Q., Zhang, X.,Wang, S.,Yu, X., Liu, Q., Liu, T. milling tool wear monitoring via the multichannel cutting force coefficients. Machines. 2024, 12, 249, https://doi.org/10.3390/machines12040249
6. Nur, R.,Yusof, N.M., Sudin, I., Nor, F.M.;, Kurniawan, D. Determination of energy consumption during turning of hardened stainless steel using resultant cutting force. *Metals.* 2021, *11*, 565, https://doi.org/10.3390/met11040565

7. Zagórski, K.; Cutting forces during milling of vertical thin-walled structures of aerospace alloys. Advances in Science and Technology Research Journal. 2023, 19(7), 197–210, https://doi.org/10.12913/22998624/203976
8. Teimouri, R., Grabowski, M., Kowalczyk, M., Skoczypiec, S. Simulation of surface roughness alternation in milling-burnishing sequence. Measurement. 2023, 218, 1–17, https://doi.org/10.1016/j.measurement.2023.113160
9. Kowalczyk, M., Tomczyk, K. Procedure for determining the uncertainties in the modeling of surface roughness in the turning of NiTi alloys using the Monte Carlo Method. Materials. 2020, 13, 1–14, https://doi.org/10.3390/ma13194338
10. Zhang, P., Moraal, J. and Li, Z. Design, Calibration and validation of a wheel-rail contact force measurement system in v-track. Measurement. 2021, 175, 1–15, https://doi.org/10.1016/j.measurement.2021.109105
11. Jin, Y., Alvarez, J.T., Suitor, E.L., Swaminathan, K., Chin, A., Civici, U.S., Nuckols, R.W., Howe, R.D. and Walsh, C.J. Estimation of joint torque in dynamic activities using wearable a-mode ultrasound. Nat. Commun. 2024, 15, 5756, 1–12, https://doi.org/10.1038/s41467-024-50038-0
12. Seo, J.W., Kim, H., Kim, J.U., Do, J.H. and Ko, J. Ground force precision calibration method for customized piezoresistance sensing flexible force measurement mat. Sensors. 2024, 24, 1–10, https://doi.org/10.3390/s24072363
13. Clark, N.C., Pethick, J. and Falla, D. Measuring complexity of muscle force control: theoretical principles and clinical relevance in musculoskeletal research and practice. Musculoskelet Sci. Pract. 2023, 64/102725, 1–7, https://doi.org/10.1016/j.msksp.2023.102725
14. del-Cuerpo, I., Mayorga, D.J., Floody, P.D., Morenas-Aguilar, M.D. and Chirosa-Ríos, L.J. Test–retest reliability of the functional electromechanical dynamometer for squat exercise. Int. J. Environ. Res. Public Health. 2023, 20, 1–13, https://doi.org/10.3390/ijerph20021289
15. Cheng, Z. and Lu, Z. Research on dynamic load characteristics of advanced variable speed drive system for agricultural machinery during engagement. Agriculture. 2022, 12/161, 1–13, https://doi.org/10.3390/agriculture12020161
16. Devine-Wright P., Peacock A. Putting energy infrastructure into place: a systematic review. Renew. Sustain. Energy Rev. 2024, 197, 1–18, https://doi.org/10.1016/j.rser.2023.114272
17. Wang S., Zhang S., Wen S. and Fernandez C. An accurate state-of-charge estimation of lithium-ion batteries based on improved particle swarm optimization-adaptive square root cubature kalman filter. J. Power Sources. 2024, 624, 1–12, https://doi.org/10.1016/j.jpowsour.2024.235594
18. Layer, E., and Gawędzki, W. Theoretical principles for dynamic errors measurement. Measurement, 1990, 8, 45–48, https://doi.org/10.1016/0263-2241(90)90077-J
19. Layer, E. and Tomczyk, K. Measurements, Modelling and Simulation of Dynamic Systems. Springer–Verlag, Berlin Heidelberg. 2010.
20. Dichev, D., Koev, H., Bakalova, T. and Louda, P. A model of the dynamic error as a measurement result of instruments defining the parameters of moving objects. Meas. Sci. Rev. 2014, 14, 183–189, https://doi.org/10.2478/msr-2014-0025
21. Tomczyk, K. Procedure proposal for establishing the class of dynamic accuracy for measurement sensors using simulation signals with one constraint. Measurement. 2021, 178, 1–8, https://doi.org/10.1016/j.measurement.2021.109367
22. Wang S., Dang Q., Gao Z., Li B., Fernandez C. and Blaabjerg F. An innovative square root - untraced Kalman filtering strategy with full-parameter online identification for state of power evaluation of lithium-ion batteries. J. Energy Storage. 2024, 104/B, 1–14, https://doi.org/10.1016/j.est.2024.114555
23. Mupona, M.I., Rosca, J.C. and Vlase, S. Modeling a milling dynamometer as a 3DOF dynamic system by stiffness identification. Appl. Sci. 2024, 14/4981, 1–19, https://doi.org/10.3390/app14124981
24. Takahei, K., Suzuki, N. and Shamoto, E. Identification of the model parameter for milling process simulation with sensor-integrated disturbance observer. Precis. Eng. 2022, 78, 146–162, https://doi.org/10.1016/j.precisioneng.2022.07.013
25. Jannifar, A., Zubir, M.N.M and Kazi, S.N. An Innovative approach for conducting experimental modal analysis (EMA) in running harmonic for structural modal identification. Measurement. 2020, 159, 1–12, https://doi.org/10.1016/j.measurement.2020.107795
26. Chi, Y., Dong, Z., Cui, M., Shan, Ch., Xiong, Y., Zhang, D. and Luo, M. comparative study on machinability and surface integrity of γ-TiAl alloy in laser assisted milling. J. Mater. Res. Technol. 2024, 33, 3743–3755, https://doi.org/10.1016/j.jmrt.2024.10.028
27. Elliott, Ch., Vijayakumar, V., Zink, W. and Hansen, R. National instruments LabVIEW: A programming environment for laboratory automation and measurement. SLAS Technol. 2007, 12/1, 17–24, https://doi.org/10.1016/j.jala.2006.07.012
28. Mohanty, B. and Stelson, K.A. Dynamics and control of an energy-efficient, power-regenerative, hydrostatic wind turbine dynamometer. Energies. 2022, 15/2868, 1–16, https://doi.org/10.3390/en15082868

29. Wang S., Gao H., Takyi-Aninakwa P., Guerrero J.M., Fernandez C. and Huang Q. Improved multiple feature-electrochemical thermal coupling modeling of lithium-ion batteries at low-temperature with real-time coefficient correction. Prot. Control Mod. Power Syst. 2024, 9/3, 157–173, https://doi.org/10.23919/PCMP.2023.000257
30. Yeh T.M. and Sun J.J. Using the monte Carlo simulation methods in gauge repeatability and reproducibility of measurement system analysis. JART. 2013, 11/5, 780–796, https://doi.org/10.1016/S1665-6423(13)71585-2
31. Song L. and Sheng G. A Two-step Smoothing Levenberg-Marquardt Algorithm for Real-time Pricing in Smart Grid. AIMS Math. 2024, 9/2, 4762–4780, https://doi.org/10.3934/math.2024230
32. Transchel R., Stirnimann J., Blattner M., Bill B., Thiel R., Kuster F. and Wegener K. Effective dynamometer for measuring high dynamic process force signals in micro machining operations. Procedia CIRP. 2012, 1, 558–562, https://doi.org/10.1016/j.procir.2012.04.099
33. Dudzik, M., Tomczyk, K. and Jagiełło, A.S. Analysis of the Error Generated by the Voltage Output Accelerometer Using the Optimal Structure of an Artificial Neural Network. 19th International Conference on Research and Education in Mechatronics. June 2018, 7–11, https://doi.org/10.1051/matecconf/201928202068
34. Nathans, L.L., Oswald, F.L. and Nimon, K. Interpreting multiple linear regression: a guidebook of variable importance. Pract. Assess. Res. Eval. 2012, 17/9, 1–19, https://doi.org/10.4159/harvard.9780674063297.c1
35. Tomczyk, K. and Kowalczyk, M. Accuracy assessment of charge-mode accelerometers using multivariate regression of the upper bound of the dynamic error. Energies. 2023, 16/23, 1–12, https://doi.org/10.3390/en16237784
36. Cui J. and Yi G.Y. Variable selection in multivariate regression models with measurement error in covariates. J. Multivar. Anal. 2024, 202, 1–18, https://doi.org/10.1016/j.jmva.2024.105299
37. Tomczyk, K. and Kowalczyk, M. Assessment of uncertainties when determining the upper bound on the dynamic error in the measurement of cutting forces. Measurement. 2025, 249, 1–14, https://doi.org/10.1016/j.measurement.2025.116997
38. Data Sheet for the Kistler Dynamometer of type 9257B: https://www.kistler.com/INT/en/cp/multi-component-dynamometers-9257b/P0000675 (accessed: 25 May 2025).